

Ceramic Electrolytes in the $\text{CeO}_2\text{-Gd}_2\text{O}_3\text{-SrO}$ System – Preparation, Properties and Application for Solid Oxide Fuel Cells

Magdalena Dudek

AGH-University of Science and Technology, Faculty of Fuels and Energy, 30-059 Kraków, al. Mickiewicza 30, Poland

*E-mail: potoczek@agh.edu.pl

Received: 8 February 2012 / Accepted: 17 March 2012 / Published: 1 April 2012

Both Pechini method (A) and hydrothermal treatment of co-precipitated gels (B) solutions were used to synthesize nanopowders of $\text{Ce}_{0.8-x}\text{Gd}_{0.2}\text{Sr}_x\text{O}_{2-\delta}$ for $0 < x < 0.1$ solid solutions. All resulting powders and sinters were found to be cubic ceria-based solid solutions. The results of hardness, fracture toughness and bending strength measurements are reported for the sintered samples of the $\text{CeO}_2\text{-SrO-Gd}_2\text{O}_3$ system. The electrical properties of ceria-based solid solutions were studied by a.c impedance spectroscopy in the temperature range 200-700°C. It was found that incorporation of a small amount of cation Sr^{2+} into solid solution $\text{Ce}_{0.8-x}\text{Gd}_{0.2}\text{Sr}_x\text{O}_{2-\delta}$ $0 < x < 0.03$ allowed an increase, in the ionic conductivity of a $\text{Ce}_{0.8}\text{Gd}_{0.2}\text{O}_{2-\delta}$ oxide electrolyte. Selected materials from the $\text{CeO}_2\text{-Gd}_2\text{O}_3\text{-SrO}$ system were tested as oxide membranes in solid oxide fuel cells operating in the temperature range 500-800°C. The higher current and power density received from IT-SOFCs with a new electrolyte $\text{Ce}_{0.78}\text{Gd}_{0.2}\text{Sr}_{0.02}\text{O}_{2-\delta}$ were recorded and compared to the same IT-SOFC involving $\text{Ce}_{0.8}\text{Gd}_{0.2}\text{O}_{2-\delta}$ as an electrolyte.

Keywords: solid oxide electrolytes, ceria-based solid solutions, co-doping, solid oxide fuel cell

1. INTRODUCTION

Ceria – based solid solutions with the formula $\text{Ce}_{1-x}\text{M}_x\text{O}_{2-\delta}$, $\text{M} = \text{Gd}, \text{Sm}, \text{Y}$ and $0.1 < x < 0.3$ are seen as potential candidates for application as oxide electrolytes for solid oxide fuel cells (SOFCs) operating in the temperature range 600-800°C [1-4]. The main drawback of ceria – based electrolytes is the increase in electronic conductivity in materials under low oxygen partial pressure (below 10^{-10} atm) at 800°C [5]. It has been reported that a reduction of ceria can be ignored at lower temperatures around 600-700°C. However, such temperatures are not suitable for singly doped ceria as an electrolyte in a

SOFC or other devices due to high electrical resistance [6,7]. Structural modification of ceria-based solutions by co-doping is one possible way to increase, the ionic oxide conductivity of ceria-based electrolytes in the intermediate temperature range (500-700°C). Materials co-stabilized with Gd₂O₃ or Sm₂O₃ and other trivalent cations such as La³⁺, Nd³⁺, Y³⁺, Bi³⁺, Nd³⁺ or divalent cations Ca²⁺, Mg²⁺, Sr²⁺, depending on chemical composition, have generally improved ionic conductivities, although in some cases a deterioration in ionic conductivity or increased electronic conductivity have been observed [8-12]. The incorporation of co-doped ceria electrolytes into IT-SOFC induced higher power and current densities from this cell compared with the same SOFC utilized as an oxide membrane single doped ceria Ce_{1-x}M_xO_{2-δ}, M = Gd, Sm, Y and 0.1 < x < 0.3 [13-15].

There is growing interest in direct carbon fuel cell technology, which has allowed us to directly convert the chemical energy of carbon fuel into electricity, without burning and the emission of toxic and greenhouse gases. All the work on DCFC fuel cells is aimed at a practical and economically feasible conversion of carbonaceous solids (coal, biomass, municipal solid waste, char, etc.) directly into electric power [16-19].

The present work examines how the preparation conditions of co-doped ceria solid solutions in the CeO₂-Gd₂O₃-SrO system influences the structure and microstructure of the samples and then electrolytic properties. The practical aim of such results is obtained ceramic oxide electrolyte, which could be applied in solid oxide fuel cells fed with different types of fuel.

2. EXPERIMENTAL

The starting materials were: Ce(NO₃)₃·6H₂O, Gd(NO₃)₂·6H₂O (99.9 %), Sr(NO₃)₂·4H₂O citric acid and ethylene glycol (99.9% Aldrich). The reagents were mixed in distilled water in order to prepare pure CeO₂, ceria-based solid solutions with the formula Ce_{0.8-x}Gd_{0.2}Sr_xO_{2-δ}, 0 < x < 0.1. To examine how the applied method of powder preparation influences the electrolytic properties of the samples, solutions containing the relevant cations were divided into two parts. The Pechini process was applied as method (A). Citric acid and ethylene glycol were added to the nitrate solutions. The solutions were then evaporated at 70°C to obtain hard gels. They were finally calcined at 900°C for 1h and then rotary-vibratory milled by zirconia grinding media in dry ethanol.

Method (B) involved hydrothermal treatment of co-precipitated ceria-gels under autogeneous water pressure at 240°C for 6h to synthesize of the CeO₂-based nanopowders. The same nitrate solutions as in method A were used as starting materials. A concentrated (4 M) sodium hydroxide solution free of carbonates was applied as the precipitating agent. Common solutions involving Gd³⁺, Ce⁴⁺ or (Gd³⁺ and Sr²⁺) cations respectively were introduced in drops into a vigorously stirred NaOH solution to co-precipitate the ceria-based powders. The final pH was carefully adjusted to a value of 9.6-9.7 and the slurry was hydrothermally treated for 4 h at 240°C in the mother NaOH environment under autogeneous water vapour pressure. The powders were washed with a water solution of ammonium nitrate and ammonia at the appropriate pH to completely remove sodium and chloride ions. The powders were also washed with isopropyl alcohol three times and dried at room temperature.

The granulated powders were isostatically pressed under 200 MPa with a 5 % wax-water

emulsion added as a lubricant. The pellets were sintered for 2 h at 1500°C (method A) or 1250°C-2h (method B). A heating rate of 2°C/min, up to 450°C and 6°C/min up to the maximum temperature was applied to avoid differential sintering due to powder agglomeration and temperature gradients in the samples, and also to slowly remove the gaseous products of the evaporation and decomposition of the liquid additives introduced.

2.1 Methods

The phase composition of all powders and sintered bodies were identified by X-ray diffraction analysis based on the ICDD data base. XRD measurements were done using Panalytical X'Pert Pro system with monochromatic Cu K_α radiation. The lattice parameters of the identified phases were determined using the Rietveld refinement method. The mean crystalline size (d_{hkl}) of the CeO₂-based powders was calculated according to the Scherrer formula. Specific surface areas were measured by multipoint nitrogen adsorption at -196°C (Quantachrome Nova 1200). The BET adsorption model was used to calculate particle sizes. Green samples were characterized by pore size distribution measurements (Quantachrome, PoreMaster). Transmission electron microscopy (AEM CM20 Philips) combined with EDS was used to characterize the morphology and chemical composition of the Ce_{1-x}Gd_{0.2}Sr_xO_{2-δ} (0 < x < 0.1) solid solution powders.

Scanning electron microscopy (SEM) equipped with an Energy-Dispersive X-ray analyzing system (EDX) was used for the observation of fractures in etched sinters, which were recorded with a FEI NOVA NanoSEM 200 equipped with a BSE detector. The numerical analysis of SEM microphotographs (VisiLog4 program Noesis), taken of the polished and thermally etched surfaces, was applied to measure the microstructural parameters quantitatively. The apparent density of the sintered bodies was measured by the Archimedes method.

Fracture toughness and hardness were measured by Vickers indentation using Future Tech (Japan) equipment. In the former case, a loading force of 4.90 N and in the latter of 9.81 N imposed every 10 s was applied. No cracks occurred when the lower load was used. The Palmqvist crack model [20] was used to calculate fracture toughness K_{Ic} . The bending strength (B_s) of samples of 4 mm x 4 mm x 45 mm in size was measured by a three – point method using a distance between support rollers of 40 mm and a loading rate of 2 mm·min⁻¹. A Zwick/Roell Z150 machine was used. The samples used to determine strength, fracture toughness and hardness were polished with the proper diamond suspension and finally, with colloidal alumina [21, 22].

The ionic conductivity measurements were performed by the a.c impedance spectroscopy method in the temperature range 200-800°C in static air. Impedance spectra were recorded with an automated setup, suitable for measurements of large absolute values of impedance, which combines a Solatron 1260 Impedance/Gain Phase Analyser and a Keithley 428 Current Amplifier [23]. Impedance was measured in the frequency range 10 MHz to 0.01 Hz, with an applied AC signal of 30 mV_{rms}. Measurements were made in air in constant temperatures from 200 to 800°C in two cooling and heating cycles (5 or 10°C temperature steps, with 20 min stabilisation time before each measurement). The data acquisition program tested whether the impedance values change with time and constant

temperature. For a set of test frequencies, the impedance was measured before and after the acquiring of each spectrum. When the summed relative differences in measured impedance exceeded an assumed tolerance of 1 %, the measurements were repeated. Impedance spectra were analysed by means of the nonlinear least-squares fitting of an equivalent circuit using the computer program Firdravn [24].

The ceria-based samples were tested as solid electrolytes in two kinds of solid oxide fuel cells (SOFC). In the first case, the sintered ceria-based samples (20 mm in diameter, with a thickness of about 1.5 mm) were tested as solid oxide electrolytes in two-chamber solid oxide fuel cells. An anode (50% wt. NiO-20GDC) powder (supplied by Fuel Cell Materials, USA) was mixed with terpeneol and ethyl cellulose to form a slurry, subsequently screen-printed on the side of CeO₂-based electrolytes as the anode, which was thermally heated at 1200°C for an hour.

The La_{0.6}Sr_{0.4}Co_{0.2}Fe_{0.8}O₂ (LSCF) was selected as a cathode material. The commercial pastes LSFC, LSCF-10GDC (Fuel Cell Materials, USA) were used as starting components to obtain cathode materials.

The cathode pastes were screen-printed on to the polished surface of CeO₂-based electrolytes and were first heated at 400°C for 2 h to remove organic binders, and then finally heated at 1000°C for 4 h. In this way the complete solid oxide bottom fuel cells for tests were prepared. The following single solid oxide fuel cells were investigated



where: (20GDC), Ce_{0.78}Sr_{0.02}Gd_{0.2}O₂ (2Sr20GDC) was a 1.5 mm-thick electrolyte, LSCF-GDC was a composite cathode material composed of LSCF +5mol % Gd₂O₃ in CeO₂.

Fig. 1 illustrates the apparatus of a single SOFC cell. Humidified hydrogen (3 % H₂O) was used as a fuel and air as oxidant. The flow rate of hydrogen was about 30 ml·min⁻¹.

In the second case the 20GDC or 2Sr20GDC sintered samples were also tested as electrolytes in a solid oxide fuel cell supplied with a pure carbon fuel.

The direct electrochemical oxidation of carbon was studied using two types of electrochemical cells:



The experimental procedure for DC-SOFC tests has been similar to described previously [25]. The current – voltage (I-V) and current-power (I-P) curves of the both tested fuel cells were also measured by the cyclic voltametry (CV) method using electrochemical station Autolab connected with Booster 20A.

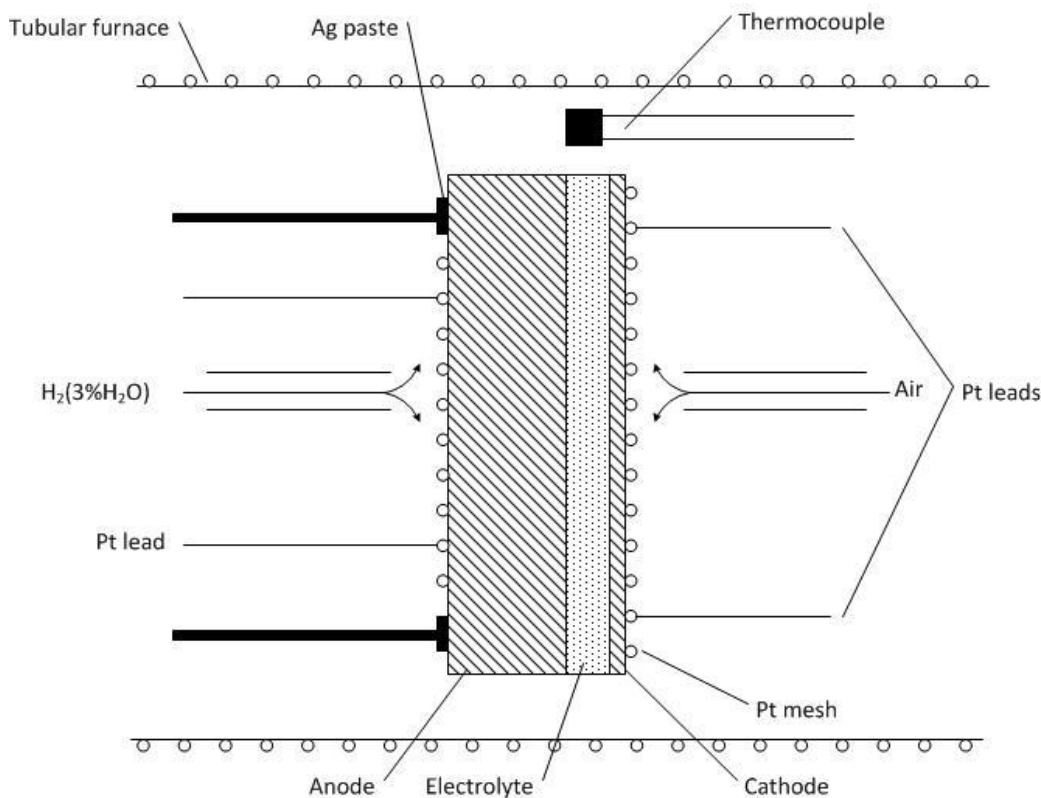


Figure 1. The apparatus for a single test of the SOFC cell

3. RESULTS AND DISCUSSION

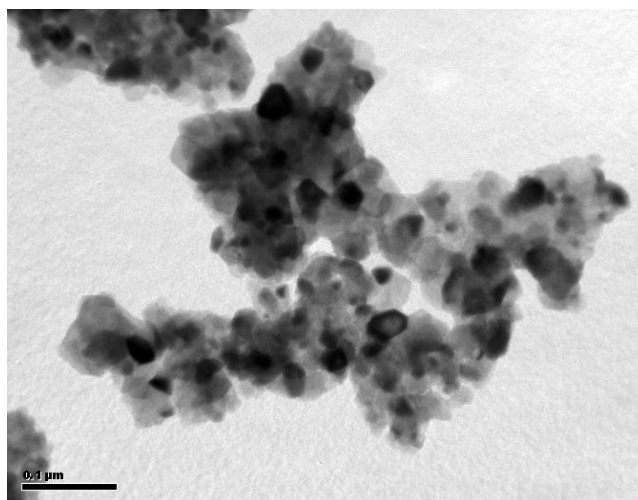
Only the cubic CeO_2 phase was evaluated by XRD diffraction analysis of all powders and samples of $\text{Ce}_{0.8-x}\text{Gd}_{0.2}\text{Sr}_x\text{O}_{2-\delta}$, solid solutions.

Table 1. Average crystalline sizes of CeO_2 -powders determined by XRD method and BET specific surface area.

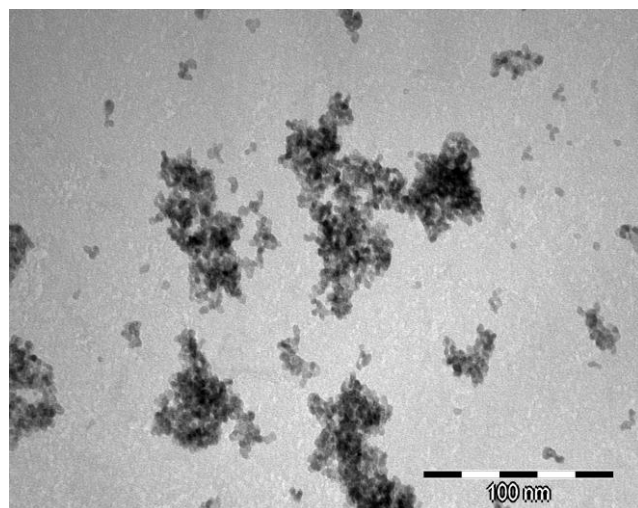
Parameter	$\text{Ce}_{0.8}\text{Gd}_{0.2}\text{O}_2$ (20GDC)	$\text{Ce}_{0.78}\text{Gd}_{0.2}\text{Sr}_{0.02}\text{O}_2$ (2Sr20GDC)	$\text{Ce}_{0.75}\text{Gd}_{0.2}\text{Sr}_{0.05}\text{O}_2$ (5Sr20GDC)	$\text{Ce}_{0.7}\text{Gd}_{0.2}\text{Sr}_{0.1}\text{O}_2$ (10Sr20GDC)
crystalline size $d_{(hkl)}$, nm	19.8 (A)	23.4 (A)	26.2 (A)	28.4 (A)
	6.3 (B)	11.2 (B)	13.4 (B)	14.2 (B)
particle size $d_{(BET)}$, nm	32.6 (A)	40.4 (A)	50.2 (A)	54.2 (A)
	9.4 (B)	13.6 (B)	15.8 (B)	18.6 (B)

The properties of CeO_2 -based powders synthesized by both methods are collected in table 1. An increase in crystalline sizes was detected in all ceria-solid solutions compared to pure CeO_2 . In the case of $\text{Ce}_{0.8-x}\text{Gd}_{0.2}\text{Sr}_x\text{O}_{2-\delta}$, where $0 < x < 0.1$ obtained by method A, the differences in particle size determined by the XRD method $d_{(hkl)}$ or $d_{(BET)}$, which are calculated from surface area measurements. This fact indicates an increase in agglomeration particle rates in powders, which was previously

mentioned during TEM observations (Fig. 2 a –b). Similar observations have been recorded for powders in $\text{CeO}_2\text{-M}_2\text{O}_3\text{-CaO}$, $\text{M} = \text{Gd}, \text{Sm}$ solid solutions [26].



A



B

Figure 2. a). TEM microphotograph of the $\text{Ce}_{0.78}\text{Gd}_{0.2}\text{Sr}_{0.02}\text{O}_{2-\delta}$ grounded powder (method A); b) TEM microphotograph of the $\text{Ce}_{0.78}\text{Gd}_{0.2}\text{Sr}_{0.02}\text{O}_{2-\delta}$ hydrothermally synthesized powder (method B)

On the other hand CeO_2 -based powders obtained by hydrothermal methods seem to be mostly composed of nanoparticles, which are isometric in shape. Among them a few elongated crystallites can also be observed, but there were none of the large needle-shaped particles typical of powders hydrothermally prepared in basic solutions [27]. After further observations of all the powders, no distinct differences in morphology were visible.

The application of mercury porosimetry allowed a determination of pore sizes (Fig. 3) in green bodies derived from $\text{Ce}_{0.78}\text{Gd}_{0.2}\text{Sr}_{0.02}\text{O}_{2-\delta}$ obtained by hydrothermal method (B) or synthesized by the Pechini method (A).

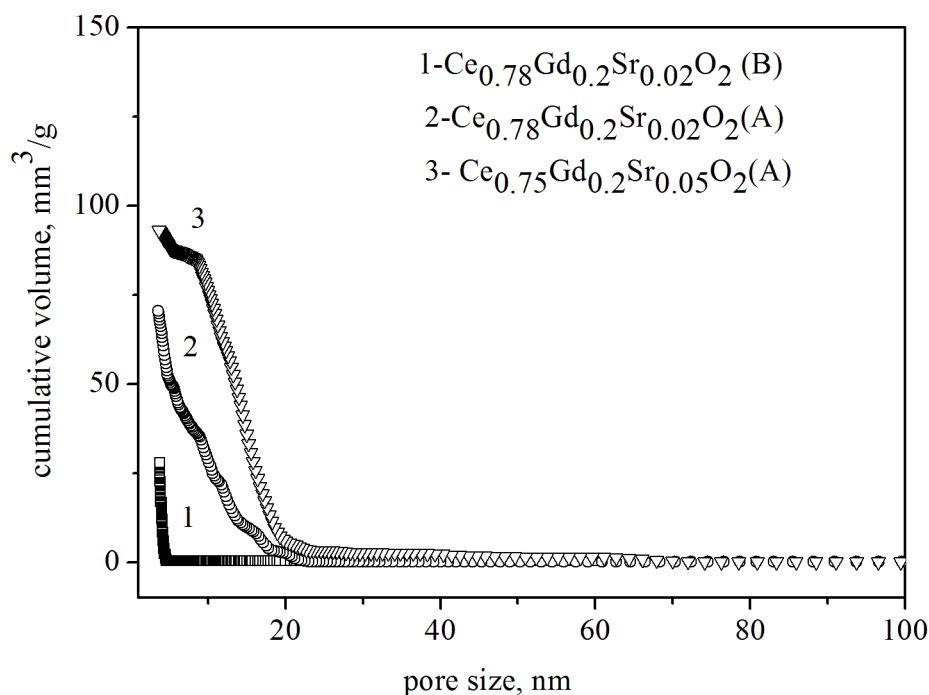


Figure 3. The pore size distribution in the isostatically pressed CeO₂-based samples.

In the case of method (B) powders compacted under an isostatic pressure of 200 MPa show an extremely narrow pore size distribution shifted to nanopores of about 6 - 7 nm in size. On the other hand, there were some differences in samples obtained from powder with the same chemical compositions obtained by powder synthesised by the Pechini process (A). The investigated samples are characterized by pores of below 100 nm. The distribution of pore dimensions seems to be narrow for both samples. However, in the case of the Ce_{0.75}Gd_{0.2}Sr_{0.05}O_{2-δ} sample there is a certain quantity of relatively larger pores in the range of 20 - 70 nm. Such pores may be formed between agglomerates of powder, while smaller ones occur between powder crystallites. The differences in pore size distributions reflect the microstructure of the samples. All the samples reached more than 96 % of theoretical density.

The typical microstructure of samples sintered at 1500°C or 1250°C for 2 h is presented in Fig. 4 a – b. This microstructural analysis allowed us to determine the average grain size distribution for pure CeO₂ and Ce_{0.8-x}Gd_{0.2}Sr_xO_{2-δ} sintered solid solution samples respectively at 1500°C or 1250°C for 2h in air. Fig. 5 presents the variations in average grain size vs. chemical composition of Ce_{0.8}Gd_{0.2}Sr_xO_{2-δ} sintered samples.

The microstructural analysis showed that the partial substitution of Ce⁴⁺ by Sr²⁺ into Ce_{0.8-x}Gd_{0.2}Sr_xO_{2-δ} solid solutions led to a small increase in average grain size compared to the initial chemical composition of the Ce_{0.8}Gd_{0.2}O_{2-δ} sample. B.Li, et al [28] also analyzed the microstructural evolution of the grain sizes of co-doped ceria solid solutions in the MgO-CeO₂-Gd₂O₃ system. They found that the addition of a small amount of MgO to Ce_{1-x}Gd_xO_{2-δ} solid solutions also led to an increase in average grain size. However, it is worth mentioning that the trends in these variations in average grain sizes are practically the same in method A and B.

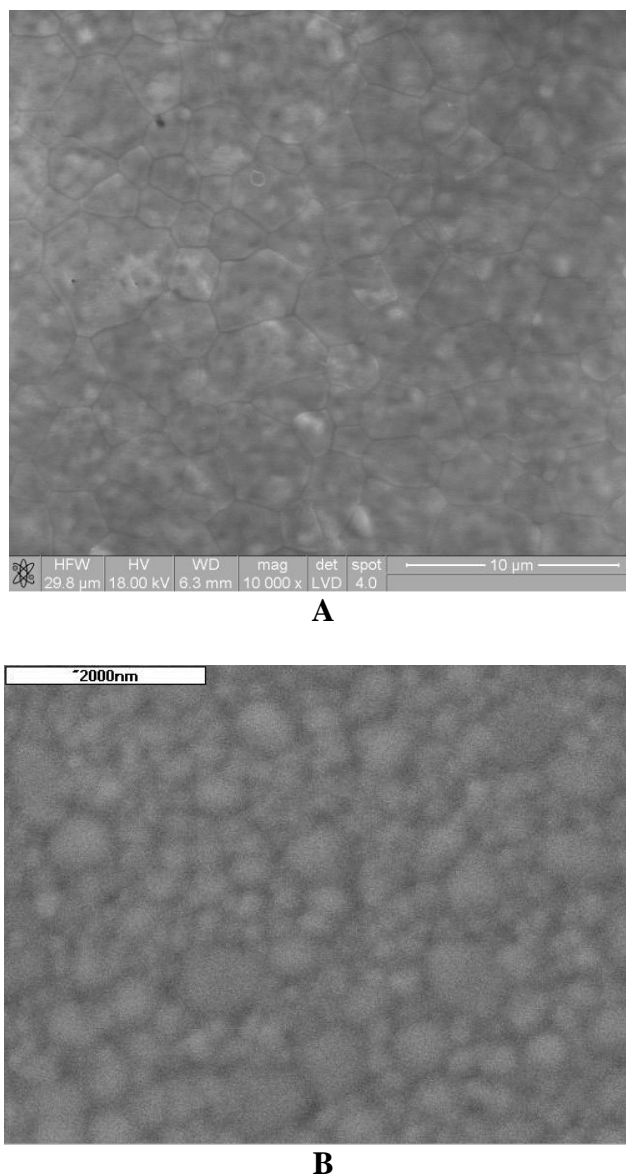


Figure 4. a) The microstructure of a $\text{Ce}_{0.78}\text{Gd}_{0.2}\text{Sr}_{0.02}\text{O}_{2-\delta}$ two-hour sintered sample at 1500°C from powder (method A); b) The microstructure of a $\text{Ce}_{0.78}\text{Gd}_{0.2}\text{Sr}_{0.02}\text{O}_{2-\delta}$ two-hour sintered sample at 1250°C from powder (method B).

The application of hydrothermal synthesis allowed us to obtain $\text{Ce}_{0.8-x}\text{Gd}_{0.2}\text{Sr}_x\text{O}_{2-\delta}$ nanopowders in ternary system $\text{CeO}_2\text{-Gd}_2\text{O}_3\text{-SrO}$ by lowering the sintering temperature of ceria-based electrolytes from 1500°C to 1250°C . This is a valuable result, which may be preferable to the application of the co-firing process of a single SOFC cell. The changes in lattice parameter a calculated for $\text{Ce}_{0.8-x}\text{Gd}_{0.2}\text{Sr}_x\text{O}_{2-\delta}$ solid solution samples are presented in Fig. 6.

The lattice parameter a of $\text{Ce}_{1-x}\text{Gd}_{0.2}\text{Sr}_x\text{O}_{2-\delta}$ solid solutions increases linearly with the increase in x content. This is due to the different ionic radii of Ce^{4+} (0.96\AA) and Sr^{2+} (1.26\AA) and agrees well with literature data [29].

Mechanical properties are also important for ceria-based materials, serving as solid oxide electrolytes, suitable for use in solid oxide fuel cells. The determined values of hardness HV , fracture

toughness K_{Ic} , bending strength (Bs) of the materials are listed in table 2.

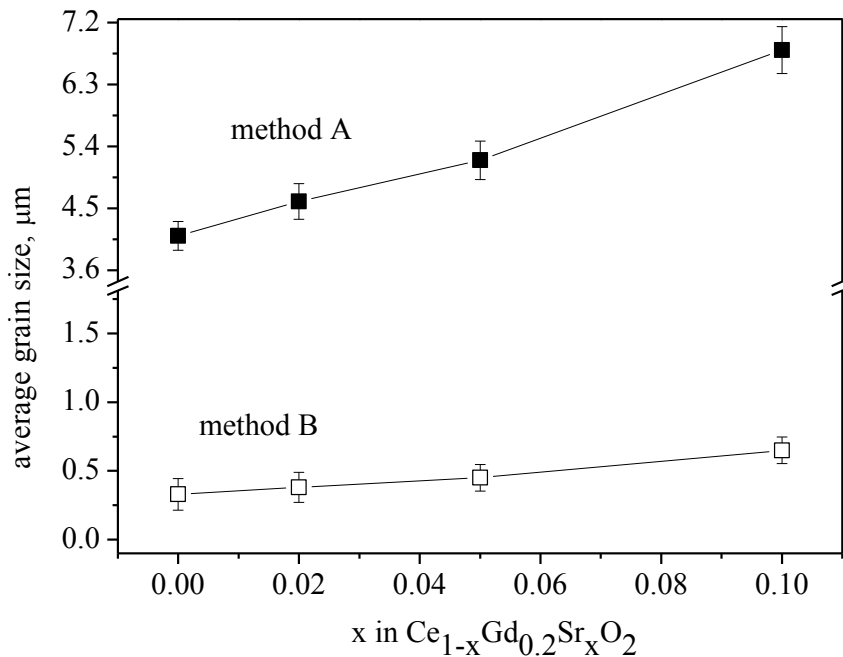


Figure 5. The dependence of an average grain size vs. the chemical composition of ceria –based samples

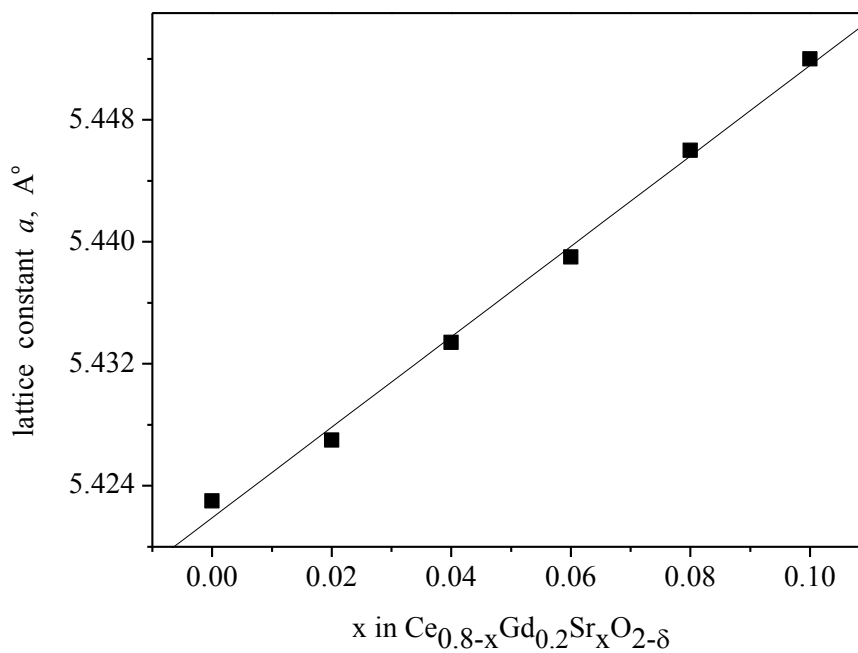


Figure 6. The changes of lattice cell parameter a calculated for $Ce_{0.8-x}Gd_{0.2}Sr_xO_{2-δ}$ sintered samples (method A).

Table 2. Hardness HV , fracture toughness K_{Ic} and bending strenght (B_s) of selected CeO_2 -based samples

Material	HV, GPa	K_{Ic} , $MPa \cdot m^{0.5}$	B_s , MPa
$Ce_{0.8}Gd_{0.2}O_2$	8.18 ± 0.32	2.38 ± 0.13	146 ± 28
$Ce_{0.78}Gd_{0.2}Sr_{0.02}O_2$	8.27 ± 0.17	2.49 ± 0.16	155 ± 19
$Ce_{0.75}Gd_{0.2}Sr_{0.05}O_2$	8.42 ± 0.14	2.54 ± 0.22	157 ± 34
$Ce_{0.8}Sm_{0.2}O_2$	8.20 ± 0.20	2.30 ± 0.14	148 ± 20
8 % mol Y_2O_3 in ZrO_2 (8YSZ)	12.83 ± 0.16	2.85 ± 0.17	230 ± 20

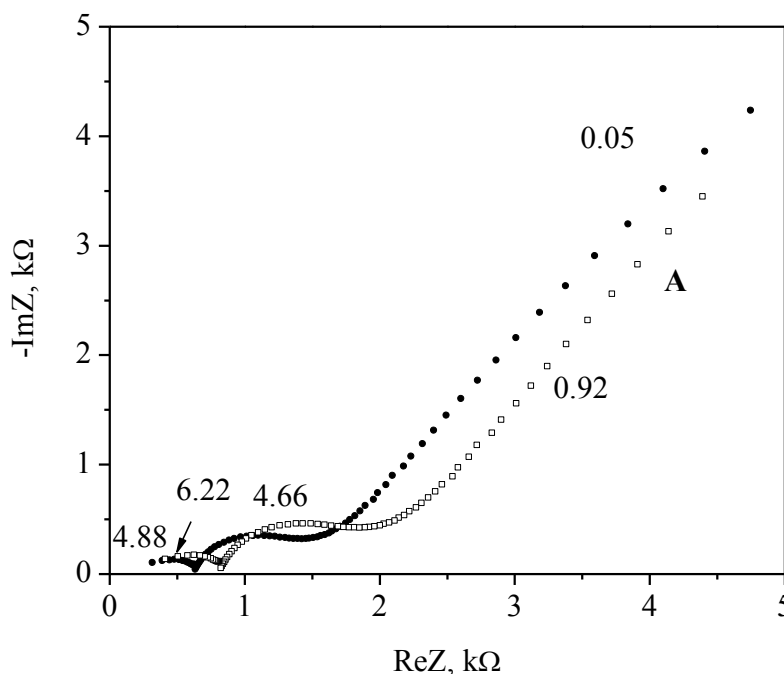


Figure 7. The impedance spectra recorded at $400^\circ C$ for a $Ce_{0.78}Sr_{0.02}Gd_{0.2}O_{2-\delta}$ sample (method A and B).

The determined values of hardness HV or fracture toughness K_{Ic} indicate that all these ceria-based materials exhibited slightly lower values for hardness and toughness compared to 8YSZ. The crack propagation observations for ceria – based samples and 8YSZ electrolyte indicated that cracks developed both along the grain boundaries and across ceria grains in the materials.

The a.c impedance spectroscopy method was applied to determine the electrical properties of singly or co-doped ceria-based samples obtained by the Pechini method (A) as well as hydrothermal treatment (B). The grain and grain boundary resistance arcs for both series of samples are well resolved up to $400^\circ C$ (Fig.7).

In this case the equivalent circuit $(R-CPE)_b-(R-CPE)_{gb}-(R-CE)_{el}$ is used to fit the impedance data to calculate bulk (R_b) and grain boundary resistance (R_{gb}). After $400^\circ C$ the bulk arc is not well resolved due to a decrease in relaxation time and it's shift towards to higher frequency regions, which

exceeds used of the equipment [30]. In this case an $R_b(R-CPE)_{gb}-(R-CPE)_{el}$ equivalent circuit is used to fit the data.

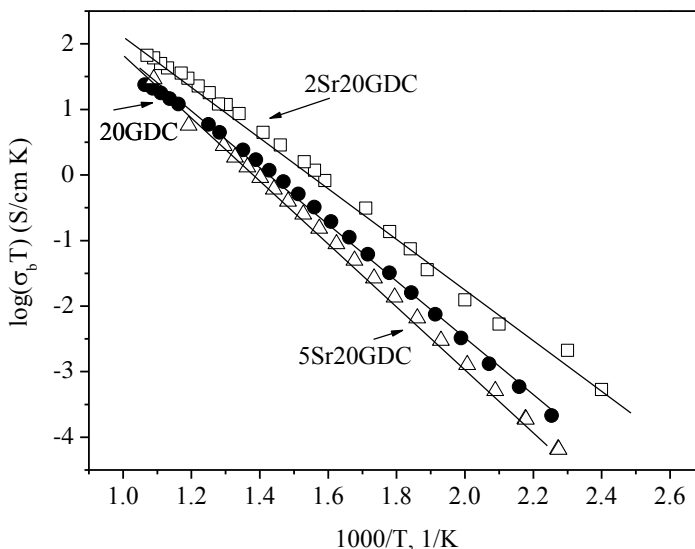
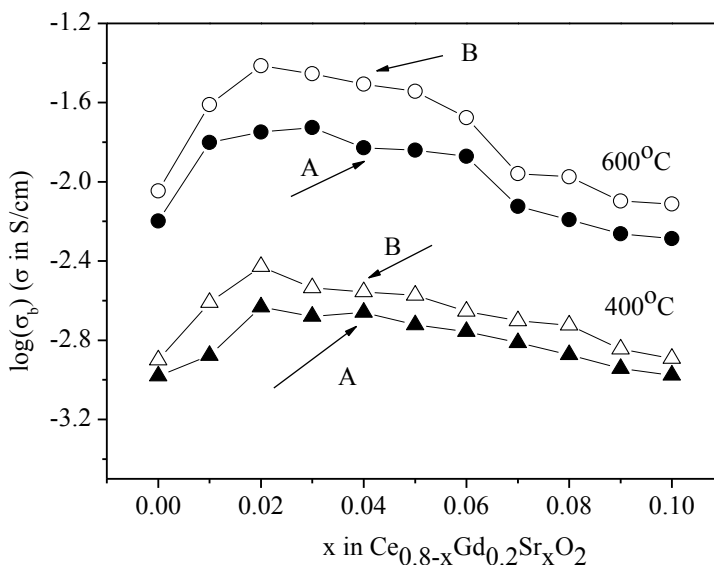


Figure 8. The $\log(\sigma_b T)$ vs. $1000/T$ determined for $Ce_{0.8}Gd_{0.2}O_{2-\delta}$ (20GDC), $Ce_{0.78}Sr_{0.02}Gd_{0.2}O_{2-\delta}$ (2Sr20GDC) and $Ce_{0.75}Sr_{0.05}Gd_{0.2}O_{2-\delta}$ (5Sr20GDC) samples (method A).

The Arrhenius plot of bulk for $Ce_{0.78}Gd_{0.2}Sr_{0.02}O_{2-\delta}$ (2Sr20GDC), $Ce_{0.75}Sr_{0.05}Gd_{0.2}O_{2-\delta}$ (5Sr20GDC) and $Ce_{0.8}Gd_{0.2}O_{2-\delta}$ (20GDC) samples is shown (Fig. 8) in $\log(\sigma T)$ v.s $1/T$ coordinated. These results indicate that co-doped ceria $Ce_{0.78}Gd_{0.2}Sr_{0.02}O_{2-\delta}$ exhibit slightly higher values of bulk conductivity compared to the $Ce_{0.8}Gd_{0.2}O_{2-\delta}$ sample.

Fig. 9 a – b. show the dependence of the bulk or grain boundary conductivity of $Ce_{0.8-x}Gd_{0.2}Sr_xO_{2-\delta}$ solid solutions vs. strontium concentration. The data was recorded at 400 and 600°C.



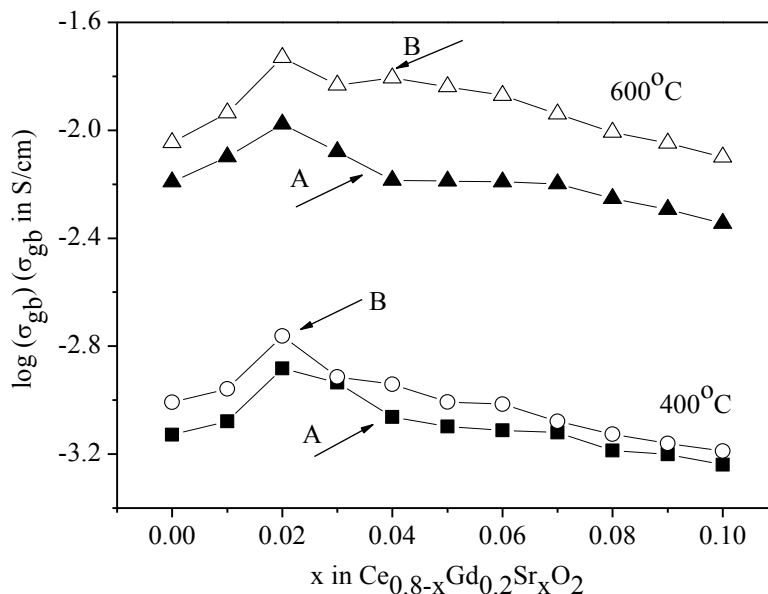


Figure 9. a) Bulk conductivity as a function of composition in Ce_{0.8-x}Gd_{0.2}Sr_xO_{2-δ} samples at 400°C and 600°C; b) Grain boundary conductivity as a function of composition in Ce_{0.8-x}Gd_{0.2}Sr_xO_{2-δ} samples at 400°C and 600°C.

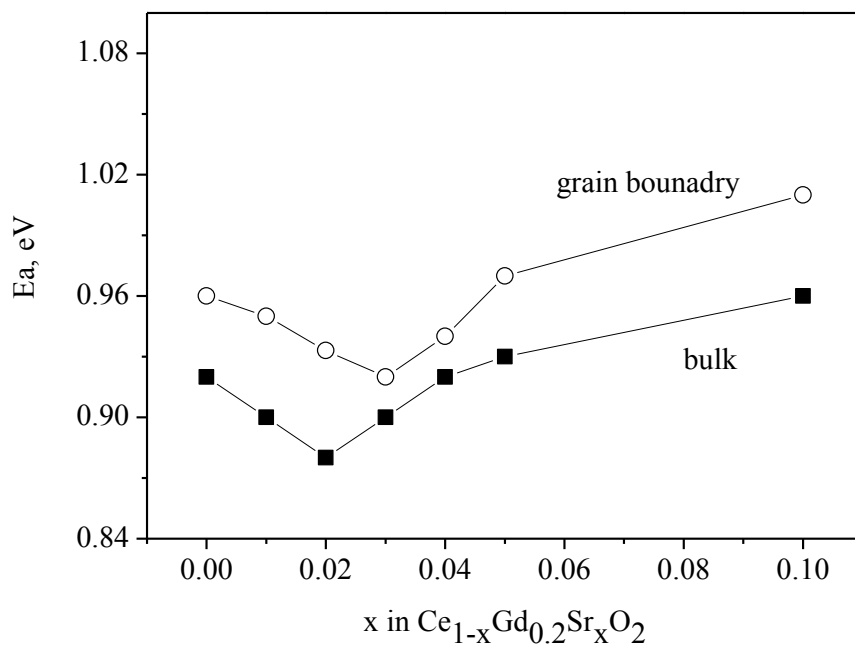


Figure 10. Activation energy of bulk and grain boundary conductivity of Ce_{0.8-x}Gd_{0.2}Sr_xO_{2-δ} samples (method A)

At a lower dopant concentration of Sr²⁺ (up to x =0.02), the bulk conductivity reaches maximum values, and then it decreases with an increasing dopant concentration.

A comparison of samples of the same composition sintered in different conditions clearly indicated that samples sintered at 1250°C exhibited higher values of bulk as well as grain boundary conductivity and then it decreases with an increasing dopant concentration.

One of the possible reasons for the higher values of the bulk conductivity of $\text{Ce}_{0.78}\text{Gd}_{0.2}\text{Sr}_{0.02}\text{O}_{2-\delta}$ solid solutions in comparison to $\text{Ce}_{0.8}\text{Gd}_{0.2}\text{O}_{2-\delta}$, could be an increase in the mobility of oxygen vacancies. The analysis of the energy activation (Fig.10) process is also indicates the minimum values, which correspond to maximum ionic conductivity (Fig.9 a-b).

The change in activation energy could be attributed to an order – disorder transition of the oxygen sublattice [31,32]. The decrease in activation energy is due to the presence of attractive interactions between cations and oxygen vacancies. Also with increasing dopant concentration levels, defects associated with oxygen vacancies and dopant cations can change from dimers to trimers and then lead to the defect clusters, consequently resulting in high binding energy, which is responsible in increase in energy activation [33].

Another problem associated with the final ceramic microstructure is the rather low conductivity of grain boundary (σ_{gb}), as compared with that of the corresponding bulk. This fact is attributed to the presence of impurities located in the grain boundary, which lower the ionic mobility. One possible solution, that has been suggested to overcome this is: decreasing grain boundary resistivity by increasing the grain sizes, i.e. lowering the GB density, or the incorporation of a controlled amount of dopants such as CaO, SrO, which could cleanse the GB of non-aequate impurities in Gd_2O_3 doped ceria [34,35].

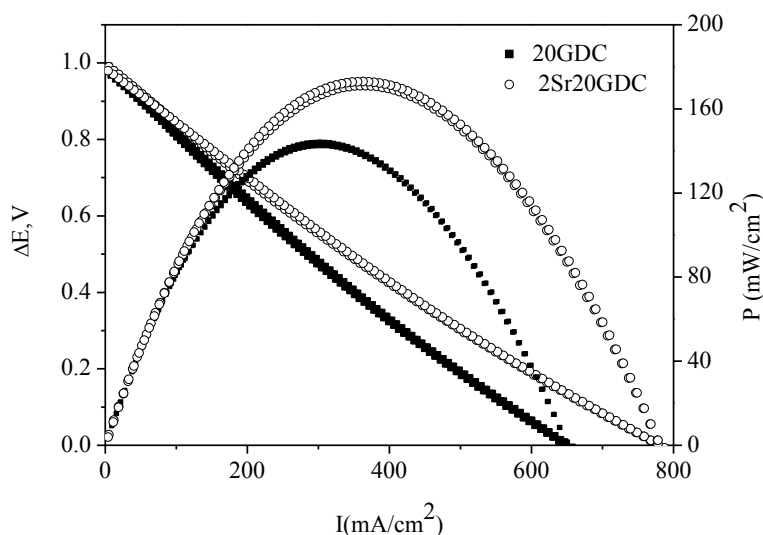


Figure 11. The family of P-I curves recorded for (20GDC) and (2Sr20GDC) samples at the temperature of 700°C (cells a, b)

P. Cho, et al [36] mentioned the diffusion induced grain boundary (DIGM) could be another possible means of improving grain boundary conductivity in CeO_2 -SrO solid solutions.

The $\text{Ce}_{0.8}\text{Gd}_{0.2}\text{O}_{2-\delta}$ and $\text{Ce}_{0.78}\text{Gd}_{0.2}\text{Sr}_{0.02}\text{O}_{2-\delta}$ samples (method B) were chosen for further investigations as components of solid oxide fuel cells filled with gaseous hydrogen or solid carbon particles as fuels. Fig. 11. shows the family of overpotential (ΔE) – current density (I) recorded for an SOFC with 20GDC (a) and 2Sr20GDC samples as electrolytes at a temperature of 700°C.

The power (P) density as well as current (I) density of an SOFC with $\text{Ce}_{0.78}\text{Gd}_{0.2}\text{Sr}_{0.02}\text{O}_{2-\delta}$ electrolyte reached higher values than the same SOFC, involving the $\text{Ce}_{0.8}\text{Gd}_{0.2}\text{O}_{2-\delta}$ electrolyte. This could be attributed to a decrease in the resistance of the cell. As can be seen, the utilization of solid oxide electrolyte with higher ionic conductivity led to a reduction in ohmic losses during IT-SOFC performance.

An important idea for direct carbon fuel cell technology is to improve the current densities and the power density drawn from this cell. In the case of solid oxide fuel cells filled with carbon powder the most important tested solid electrolyte in DC-SOFC is 8 % Y_2O_3 in ZrO_2 (8YSZ) [37-38]. Our previous investigations [25] also showed that replacing 8YSZ with an oxide electrolyte with higher ionic conductivity could be one of the possible ways of improving the performance of such cells.

The increase in current density as well as power density of a solid fuel cell filled by carbon vs. temperature is recorded. In DC-SOFC, during the direct carbon conversion, carbon dioxide (CO_2) is produced at the anode, and it can be sequestered. A competing reaction of the direct carbon conversion: $\text{C} + \text{O}_{2(\text{g})} \leftrightarrow \text{CO}_{2(\text{g})}$ (1) is the Boudouard reaction $\text{C} + \text{CO}_{2(\text{g})} \leftrightarrow 2\text{CO}_{(\text{g})}$ (2). At higher temperatures this reaction is shifted to the right side, so that carbon monoxide (CO) may be produced. This reaction is endothermic, and leads to fuel loss. Thus, to minimize this effect, we have reduced the operating temperature. In the SOFC, conventional material used as a solid oxide electrolyte is exclusively zirconia stabilized by 8% mol Y_2O_3 (8YSZ) in the temperature range 800–1000°C. In order to reduce temperature of the operating DC-SOFC down to 700°C, the ceria-based electrolytes should be utilized as oxide membranes in ceramic fuel cells.

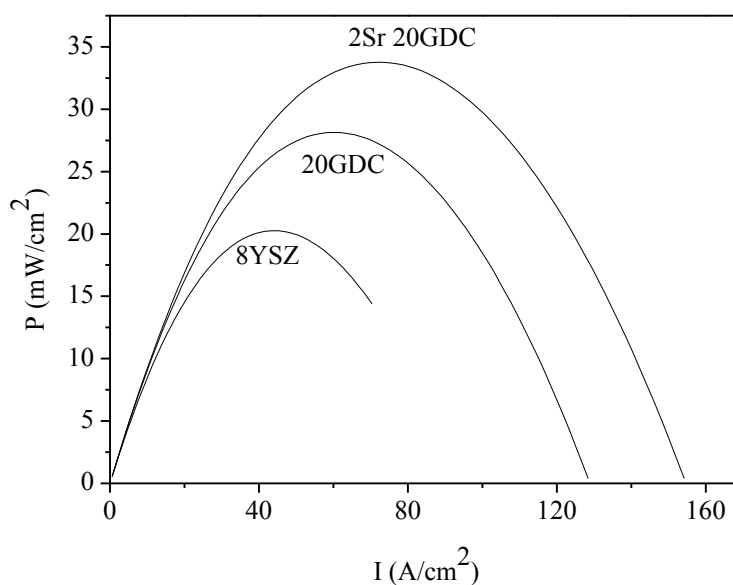


Figure 12. The family of P-I curves recorded for DC-SOFC cell (d,c) at 700°C.

Fig. 12 also shows comparable results for DC-SOFC with a 8YSZ, 20GDC or 2Sr20GDC at 700°C. As can be seen an increase in current density as well as power density comes from a DC-SOFC involving an oxide electrolyte with lower ohmic resistance. These results also indicate that a co-doped ceria electrolyte with the $\text{Ce}_{0.78}\text{Gd}_{0.2}\text{Sr}_{0.02}\text{O}_{2-\delta}$ formula seem also to be promising materials for DC-SOFC technology.

4. CONCLUSIONS

Singly-doped ceria or co-doped ceria materials $\text{CeO}_2\text{-Gd}_2\text{O}_3\text{-SrO}$, were successfully prepared both from powders obtained by the Pechini method (A) and by hydrothermal (B) synthesis. The application of ceria-based powders prepared by hydrothermal synthesis allowed a reduction in the sintering temperature of ceria-based electrolytes from 1500°C to ca. 1250°C.

It was found that the introduction of strontium into a $\text{Ce}_{0.8-x}\text{Gd}_{0.2}\text{Sr}_x\text{O}_{2-\delta}$ solid solution leads to improving of ionic conductivity compared to $\text{Ce}_{0.8}\text{Gd}_{0.2}\text{O}_2$ samples.

A direct comparison of results of ionic conductivity indicated that the better results were achieved for ceria-based samples obtained by hydrothermal method than Pechini process.

The $\text{Ce}_{0.78}\text{Gd}_{0.2}\text{Sr}_{0.02}\text{O}_{2-\delta}$ dense samples seem to be more adequate oxide electrolytes than $\text{Ce}_{0.8}\text{Gd}_{0.2}\text{O}_2$, for application of solid oxide fuel cells filled with gaseous hydrogen or a solid carbon.

ACKNOWLEDGEMENTS

This work was sponsored by the AGH-University of Science and Technology, Faculty of Fuels and Energy.

References

1. H. Inaba, H. Tagawa, *Solid State Ionics* 83 (1996) 1.
2. S. Kuharuangrong, *J. Power Sources* 171 (2007) 506.
3. J.W Fergus, *J. Power Sources* 189 (2006) 30.
4. A.Gondolini, E. Marcadelli, *Ceramic International* 37 (2011)1423.
5. J.W. Fergus, R.Hui, X.Li, D. P. Wilkinston, J.Zhnag, CRC Press London New York, USA.
6. Y.Zheng, L.Wu, H.Gu, L. Gao, *J. Alloys Compd* 486 (2009)586.
7. T.Mori, T. Ikegami, H. Yamamura, *J. Electroch. Soc.* 146 (1999) 4380.
8. M.Dudek, W. Bogusz, Ł. Zych, B. Trybalska, *Solid State Ionics* 179 (2008) 164.
9. X. Guan, H. Zhou, Y. Wang, J. Zhang, *J. Alloys Compd* 464 (2008) 310.
10. S. Ohmar, E. Wachsman, J. Nino, *Solid State Ionics* 178 (2008) 1890.
11. S.Ramesh, V. Kummar, P. Kistaih, C. Reddy, *Solid State Ionics* 181 (2010) 86.
12. S. Dikmen, *J. Alloys Compd* 491 (2010) 106.
13. Y. Ji, J.Liu, T. He, J. Wang, W. Su, *J. Alloys Compd* 389 (2005) 317.
14. J.Cheng, Q. Jiang, H. He, J. Jang, *Mat. Chemistry and Physics* 125 (2011)704
15. X. Hongmei, Y. Hongge, Ch. Zhenhua, *Solid State Science* 10 (2008) 1179.
16. S.L.Jain, Y. Nabae, B.Lakeman, K.Pointon, J. Irvine, *Solid State Ionics* 179 (2008) 1417.
17. G.A. Hackett, J.W. Zondlo, W. Stevansson, *J. Power Sources* 68 (2007) 111.
18. Y. Nabae, K.T.Pointon, J.Irvine, *Energ. Environ. Sci.* 1 (2008) 148.

19. D. Cao, G. Wang, Ch. Wang, J. Wang, T. Lu, *Int J. Hydrog Energ* 35 (2010) 1778.
20. K. Niihara, *J. Mater. Sci. Lett.* 2 (1983) 221.
21. N. Moskała, W. Pyda, *J. Eur. Ceram. Soc.* 26 (2006) 3845-3851.
22. R. Lach, K. Haberko, M.M. Bućko, M. Szumera, G. Grabowski, *J. Eur. Ceram. Soc.* 31(2011) 1889-1895.
23. J.R. Dygas, W. Breiter, *Electrochim. Acta* 41 (1996) 993.
24. J.R. Dygas, W. Breiter, *Electrochim. Acta* 44 (1999) 4163.
25. M. Dudek, P. Tomczyk, *Catal. Today*, 176 (2011) 388-392
26. M. Dudek, A. Rapacz-Kmita, M. Mroczkowska, M. Mosiałek, G. Mordarski, *Electrochim. Acta* 55 (2010) 4387.
27. W. Pyda, *Bull. Polish Academy of Sciences*. 1999 (47) 397.
28. B. Li, W. Pen, *J. Power Sources* 183(2008) 498.
29. R.P Shannon, T. Prewitt, *Acta Crystallog. Sect. B: Struct. Sci* 25 (1969) 925.
30. A.F. Orliukas, A. Kezionis, E. Kazakevicius, *Solid State Ionics*, 176 (2005) 2037.
31. J.A Kilner, *Solid State Ionics* 129 (2000) 13.
32. P.J. Schlichta, *Solid State Ionics* 28-30 (1988) 480.
33. F. Ye, T. Mori, D.R. Ou, A. N. Cormack, *Solid State Ionics* 180 (2009) 1127.
34. F. Ye, T. Mori, D. R. Ou, M. Takahashi, J. Zou, J. Drennan, *J. Electrochem. Soc.* 154 (2007) B180.
35. P. Seok, S. B. Lee, D.S. Kim, J. H. Lee, D. Kim, H. Park, *Electrochem. Solid-State Lett.* 9 (2006) A399.
36. P. Cho S. Park, J. Kim, H. Do, *Solid State Ionics* 181(2010) 1420.
37. Ch. Li, Y. Shi, N. Cai, *J. Power Sources* 196 (2011) 754.
38. J.P Kim, H. Lim, Ch.H. Jeon, Y.J. Chang, K.-N. Koh, S. M. Choi, *J. Power Sources* 195 (2010) 7568.
39. S. L. Jain, Y. Nabae, B. J. Lakeman, K. D. Pointon, J. T.S. Irvine, *Solid State Ionics*, 179 (2008) 1417.